Tomographic Profiling of the Structure of a Snow Pack at X-/Ku-Band using SnowScat in SAR Mode

Othmar Frey
Gamma Remote Sensing /
Earth Observation & Remote Sensing, ETH Zurich
Switzerland
Email: frey@gamma-rs.ch

Charles L. Werner, Andreas Wiesmann
Gamma Remote Sensing
Switzerland
Email: {cw, wiesmann}@gamma-rs.ch

***Abstract*—The SnowScat device, a fully-polarimetric scatterometer originally designed to measure the radar cross-section of snow at a frequency range from 9.2 to 17.8 GHz (X-band to Ku-band), has recently been extended towards a high-resolution tomographic measurement mode. Such tomographic profiling observations provide further insights into the complex electromagnetic interaction within snowpacks, e.g., by revealing different layers, such as melt-freeze crusts, inside the snowpack. In this contribution, we report first results from an initial tomographic measurement campaign carried out at a test site in Davos, Switzerland, in winter 2014/2015.**

***Index Terms*—SnowScat, microwave remote sensing, snow, tomography, tomographic profiling, SAR tomography, scatterometer, X-band, Ku-band, European Space Agency, ESA.**

I. Introduction

The SnowScat device is a fully-polarimetric scatterometer that has originally been designed to measure the radar cross-section of snow at a frequency range from 9.2 to 17.8 GHz (X-band to Ku-band) [1]–[4] (similar measurements using a GB-SAR at X-band and Ku-band were also reported in [5]).

Recently, a modification of the measurement setup extending the capabilities of the SnowScat device towards *tomographic profiling* of snowpacks was implemented and tested. This extension aims at enhancing the SnowScat device in order to better respond to the ESAC recommendations which were made on the deselected CoReH2O candidate following the user consultation meeting in March 2013 for the 7th Earth Explorer mission. Such new capability allows for performing high-resolution tomographic profiling observations that may provide further insights into the complex electromagnetic interaction within snowpacks.

When operated in the tomographic profiling mode, the SnowScat device is subsequently moved along a rail in the direction orthogonal to the mean look direction of the antennas. Thus, a synthetic aperture is formed in elevation direction, which leads to the tomographic profiling capability. The resolution in azimuth direction is determined by the (frequency-dependent) beamwidth of the SnowScat antenna. Consequently, the azimuth resolution also decreases as a function of the range distance. The new hardware setup, as shown in Fig. 1, supports both modes, the original scatterometer mode, and the new tomographic profiling mode. Thus, the tomographic measurement concept of SnowScat is somewhat different from a similar ground-based tomographic experiment, reported in [6], [7], in the sense that no synthetic aperture is formed in azimuth direction. Another tomographic profiling approach akin to the SnowScat setup was presented in [8].

TABLE I
System specifications of the SnowScat device after the system update for tomographic profiling

Frequency	SFCW from 9.2 to 17.8GHz
Incidence angle	-40^o to 110^o (used: 45^o)
Azimuth angle	-180^o to 180^o (used: 0^o)
Sampling spacing	0.04 m
Number of samples	50
Synth. aperture length	1.94 m
3dB res. (stripmap m.)	0.15 m
Power	230V, max $\sim$ 60W
Weight	$\sim$ 40 kg
Temperature range	-40^{o}C to 40^{o}C
Antennas	Dual pol, $<$ 10^o (3dB)
Antenna cross-pol	$<$ -25dB
Polarization	HH, HV, VV, VH
Dynamic range	Receiver dynamic range $>$ 80dB with the 16bit ADC
Signal bias	$<$ 0.5dB
Gain characterization	Internal calibration, calibration sphere (Ø = 25cm)
RFI	Frequency blacklist

In this paper, we (1) describe the tomographic mode of the SnowScat device including the experimental setup at the test site in Davos, Switzerland, as well as the tomographic processing approach. (2) First results are shown that validate the tomographic measurement concept in snow-free conditions, using a tomographic test target, as well as in presence of a snowpack.

II. Methods

A. Experimental setup at the test site Davos

The experimental setup implemented at the test site in Davos, Switzerland, is shown in Fig. 1. The SnowScat device is attached to a rail on a triangular truss, which again is mounted onto a scaffold (see Fig. 1(a)). The SnowScat device

(a) (b) (c)

Fig. 1. Experimental setup for initial tests of the tomographic profiling mode at the SLF-hosted test site in Davos Gadenstatt, Switzerland, in January, 2015. When operated in tomographic profiling mode, the SnowScat device is subsequently shifted along the rail, spanning a maximal synthetic aperture of 2220 mm (1940 mm in this experiment). The rail, tilted by 45 degree, is attached to a triangular truss, which again, is mounted onto a scaffold, such that the upper edge of the truss is approximately 10m above ground. The pointing direction of the SnowScat antennas is adjustable in elevation and azimuth. Three artificial targets were placed on the ground: A slightly tilted (15 deg) target for vertical profiling on the left, a tomographic target with its vertical array of spheres in the middle, as well as an additional calibration sphere on the right. (a) Close-up of the SnowScat device while acquiring data in the tomographic profiling mode. (b) Overview of the entire measurement setup. (c) Close-up of the SnowScat tomographic test target.

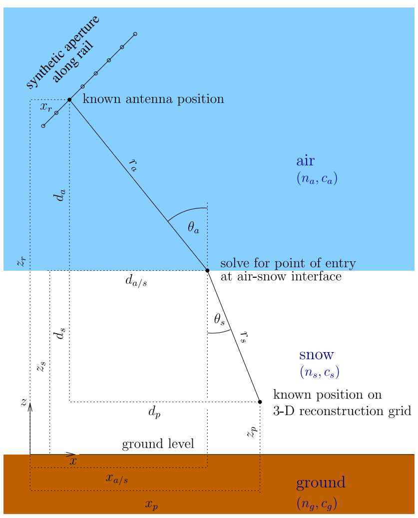

Fig. 2. Sketch of tomographic acquisition scenario of the SnowScat device for probing a snow layer. The sketch shows a ray path (and its associated defining geometric parameters) between an antenna position along the rail and a specific position on the 3-D reconstruction grid for the simplified condition where both the snow layer and the atmosphere are homogenous; i.e. refraction only occurs at the air-snow interface. This condition is assumed as an initial state for the iterative solution of the focusing problem where other refractive layers may be identified.

can be moved along this rail (tilted by 45 degree) within a maximal total synthetic aperture length of 2.22m (1.94m in the experiment presented here). In addition, the antenna pointing direction can be adjusted in elevation and azimuth (as in the original SnowScat design). The results presented in this paper were acquired at an incidence angle of 45 degree, and 0 degree azimuth angle (i.e. within the nadir/elevation plane). The centre of the synthetic aperture is located approximately 7.5m above ground. At this central position the SnowScat device is pointing at the centre of the tomographic target, assuming an incidence angle of 45 degree. Table I summarizes the system parameters of the SnowScat device.

B. Tomographic test target

A tomographic test target—an array of eight spheres vertically aligned on a carbon tube—has been placed in the field of view of the SnowScat device. The tomographic test target has been used to characterise the focusing performance of the aperture synthesis. In addition, it also serves as a reference for the data acquisition under snow conditions. Fig. 1(b) gives an overview of the measurement setup under snow conditions. Fig. 1(c) shows a close-up view of the tomographic test target.

C. TDBP-based tomographic profiling

The vertical snow profiles are obtained by a time-domain back-projection (TDBP) approach [9], [10], i.e. basically, through aperture synthesis along the elevation direction.

The TDBP processing employed, so far, is essentially a ray-tracing approach that takes into account a simplified refraction model assuming one homogeneous snow layer with refraction occurring at the air/snow interface. The calculation of the point of entry at the air/snow interface is based on the trigonometric relationships as depicted in Fig. 2. A virtual range distance R_v is obtained iteratively based on the incidence angle θ, the angle of refraction θ_S, the refractive index n_s, and the different phase velocities c (in air) and v_S (in the snow volume). The TDBP aperture synthesis along the elevation direction can then be written as:

$$v(\vec{r}_i) = \sum_{k=1}^{M} g_k[R_v(\vec{r}_i, \vec{r}_k, n_s)] \cdot \exp[i\ 4\pi/\lambda R_v(\vec{r}_i, \vec{r}_k, n_s)] \ , \tag{1}$$

where $\vec{r}_i$ is the 3-D pos. vector of the target location for which the tomographic inversion is performed, $\vec{r}_k$ is the 3-D pos. vector of the antenna phase centre at position k within the synthetic aperture, $g_k(...)$ is the range-compressed signal at antenna position k, λ is the wavelength of the carrier signal, $R_v(\vec{r}_i, \vec{r}_k, n_s)$ is the (virtual) range distance between antenna

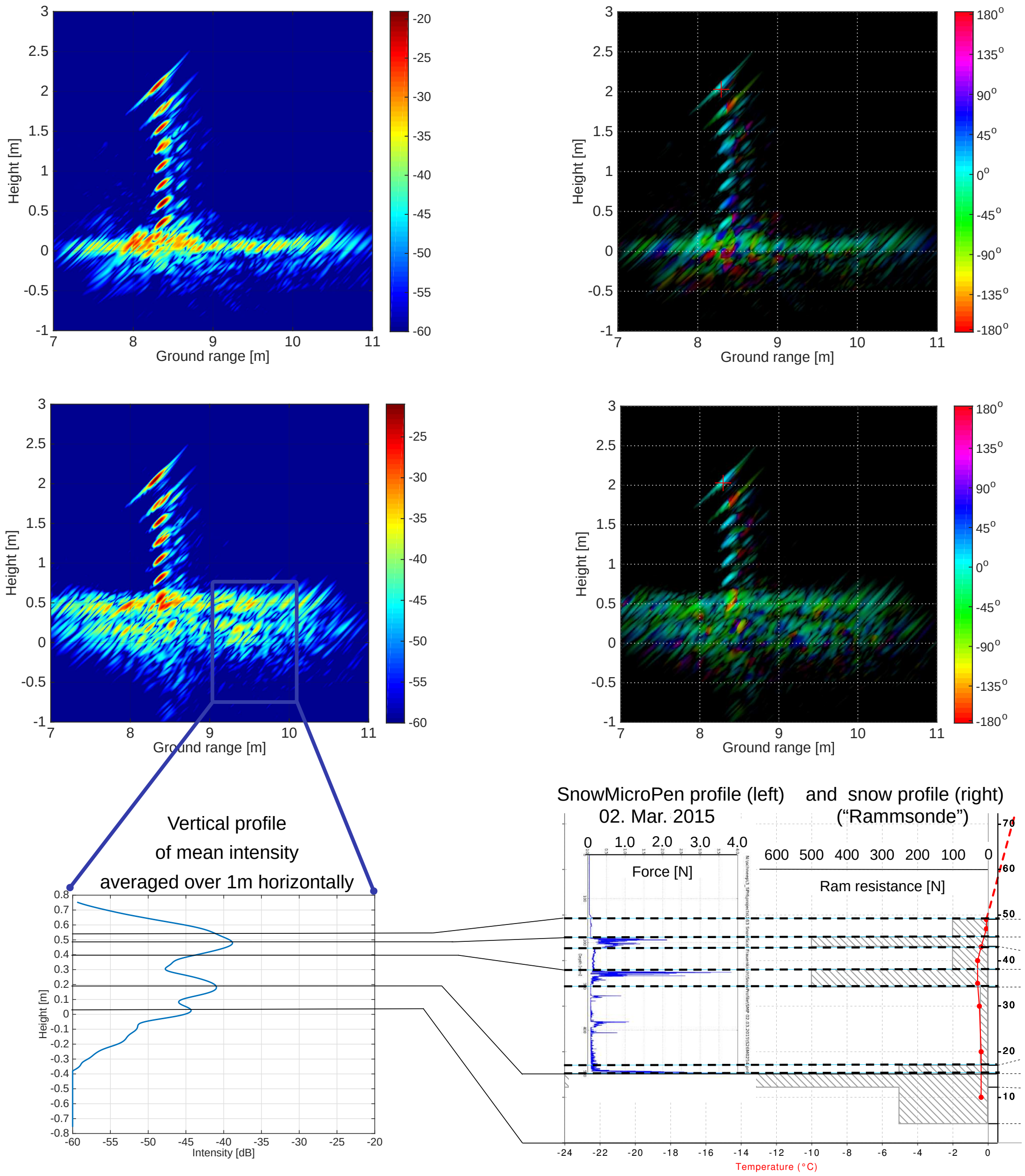

Fig. 3. Excerpt from a series of tomographic profiles of the situation including the test target with its 8 aluminium spheres at the test site in Davos, Switzerland, during winter 2014/2015. **Top row, left**: Intensity plot of the HH channel of the reference case under **snow-free condition**, acquisition date: 14. Nov. 2014. Only the surface of the meadow and the backscattering of the metal spheres of the tomographic test target are visible. Each 1-look image was obtained from 50 measurements along the rail. Aperture synthesis was performed by a time-domain back-projection approach taking into account a simple refraction model. **Top row, right**: Phase of the complex polarimetric coherence between the co-polar channels HH and VV, displayed in combination with the HH intensity in a HSV colour scheme. Hue: phase of the complex polarimetric coherence. Saturation: is unaltered and set to full saturation. Value: brightness varies according to the measured intensity in decibel. **Middle row**: Intensity plot of the HH channel (left) and phase of the complex polarimetric coherence over intensity **under snow condition** (right). Acquisition date : 03. March 2015, acquisition time: 21:01h - 23:43h, snow height measured (at SLF2 station): 60-65 cm, air temperature: -4^o - -3^o (below melting point). **Bottom row**: On the left, a vertical profile of mean intensity averaged over 1 m horizontally (blue rectangle) is shown. The 1-D vertical profile is also compared to in-situ snow profile measurements taken a day earlier, shown on the right-hand side. Two of the three main melt-freeze crusts/ice layers, and also the ground level can be identified in the tomographic snow profile.

position k and the location $\vec{r}_i$ using the simple refraction model, and $v(\vec{r}_i)$ is the focused signal at location $\vec{r}_i$.

III. Results

In Fig. 3, tomographic profiles obtained by TDBP-focusing of 50 SnowScat radar echoes are shown: Measurements of the tomographic test target with its 8 aluminium spheres, the ground surface, and a **snowpack** were taken at the test site in Davos, Switzerland.

On the left, 1-look tomographic profiles (HH channel) of the situation are shown under snow-free and snow-covered

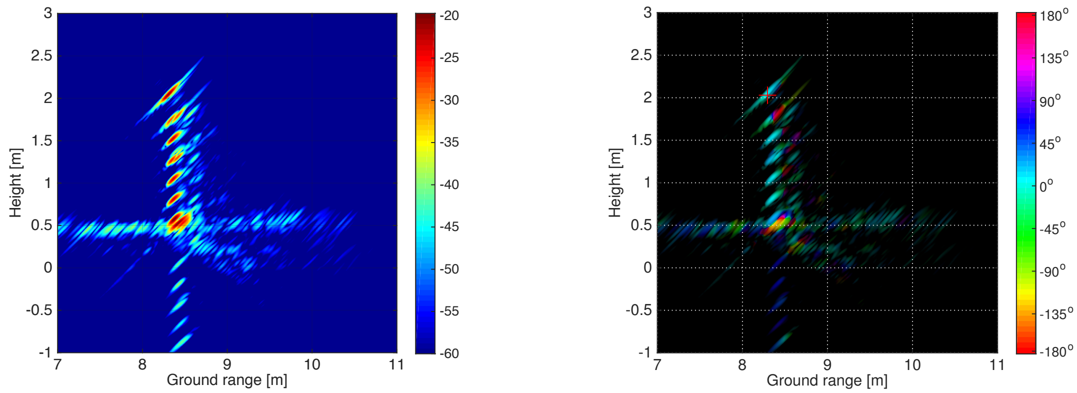

Fig. 4. Special case: data acquisition under **melted snow surface condition**. Acquisition date: 15. Feb. 2015, acquisition time: 11:15h - 15:05h, snow height measured (at SLF2 station): 45-50 cm, air temperature: 4.3^o - 10^o. Virtually no penetration into the snow is observed. Instead, double bounce (at the air/snow interface) and triple bounce (snow surface, sphere, snow surface) scattering artefacts ("ghost targets" below the ground) are present. The phase values of the polarimetric coherence of the co-polar channels HH and VV at the location of the double bounce and the triple bounce ghost targets, confirm this observation, as shown in the plot on the right-hand side.

condition. Aperture synthesis was performed by a TDBP approach as described in Section II-C. On the right, the phase of the complex polarimetric coherence of the co-polar channels HH and VV, displayed in combination with the HH intensity in a HSV colour scheme, are shown (see Fig. caption for details). A distinct (non-zero) phase difference between the co-polar channels is observed for both, back-scattering from the pasture (snow-free condition) and also for back-scattering under snow-conditions. For the data acquisition under snow condition (03. March 2015) a vertical profile of mean intensity averaged over 1 m horizontally is also given. In addition, in-situ snow profile measurements were taken on 02. March 2015 (see Fig. 3 bottom right)).

In Fig. 4, a special case is shown: the data was acquired under melted snow surface condition. Virtually no penetration into the snow is observed. Instead, "ghost targets" are visible due to double bounce and triple bounce scattering. The phase values of the polarimetric coherence of the co-polar channels HH and VV at the location of the ghost targets confirm this observation.

IV. Discussion

The basic measurement concept for the SnowScat tomographic profiling mode was successfully verified: The 8 metal spheres are well focused and can easily be distinguished in the tomogram under snow-free conditions. In addition, substantial backscattering signal is also obtained from the base of the test target as well as from the ground. Both features appear well-focused and are well-distinguishable in the tomogram.

A comparison of the tomographic profiles under snow conditions with the in-situ snow profiles indicates that two of the three main melt-freeze crusts/ice layers, and also the ground level can be identified in the tomographic snow profile.

The phase plots of the polarimetric coherence show distinct non-zero phase that reveal polarisation-dependent scattering for both the grass land and the snow-volume above grass land. This, so far rather qualitative, confirmation of anisotropic scattering is one of the major points requiring further analysis.

Acknowledgment

This work was partly conducted in the frame of ESA/ESTEC Contract No. 20716/06/NL/EL CCN3, "Enhancement of SnowScat for tomographic and vertical profiling observation capabilities". M. Schneebeli and A. Macfarlane at SLF, Davos, Switzerland are gratefully acknowledged for managing the test site and for providing in-situ measurements of the snowpack.

References

[1] A. Wiesmann, T. Strozzi, C. L. Werner, U. Wegmuller, and M. Santoro, "Microwave remote sensing of alpine snow," in *Proc. IEEE Int. Geosci. Remote Sens. Symp.*, July 2007, pp. 1223–1227.

[2] C. L. Werner, A. Wiesmann, T. Strozzi, M. Schneebeli, and C. Matzler, "The SnowScat ground-based polarimetric scatterometer: Calibration and initial measurements from Davos Switzerland," in *Proc. IEEE Int. Geosci. Remote Sens. Symp.*, July 2010, pp. 2363–2366.

[3] A. Wiesmann, C. L. Werner, T. Strozzi, C. Matzler, T. Nagler, H. Rott, M. Schneebeli, and U. Wegmuller, "SnowScat, X- to Ku-band scatterometer development," in *Proc. ESA Living Planet Symposium*, June 2010.

[4] A. Wiesmann, C. Werner, C. Matzler, M. Schneebeli, T. Strozzi, and U. Wegmuller, "Mobile X- to Ku-band scatterometer in support of the CoRe-H2O mission," in *Proc. IEEE Int. Geosci. Remote Sens. Symp.*, vol. 5, July 2008, pp. 244–247.

[5] K. Morrison, H. Rott, T. Nagler, H. Rebhan, and P. Wursteisen, "The SARALPS-2007 measurement campaign on X- and Ku-band backscatter of snow," in *Proc. IEEE Int. Geosci. Remote Sens. Symp.*, July 2007, pp. 1207–1210.

[6] S. Tebaldini and L. Ferro-Famil, "High resolution three-dimensional imaging of a snowpack from ground-based SAR data acquired at X and Ku band," in *Proc. IEEE Int. Geosci. Remote Sens. Symp.*, July 2013, pp. 77–80.

[7] L. Ferro-Famil, S. Tebaldini, M. Davy, and F. Boute, "3D SAR imaging of the snowpack at X- and Ku-band: results from the AlpSAR campaign," in *Proc. of EUSAR 2014 - 10th European Conference on Synthetic Aperture Radar*, June 2014, pp. 1–4.

[8] K. Morrison and J. Bennett, "Tomographic profiling - a technique for multi-incidence-angle retrieval of the vertical SAR backscattering profiles of biogeophysical targets," *IEEE Trans. Geosci. Remote Sens.*, vol. 52, no. 2, pp. 1350–1355, Feb. 2014.

[9] O. Frey and E. Meier, "3-D time-domain SAR imaging of a forest using airborne multibaseline data at L- and P-bands," *IEEE Trans. Geosci. Remote Sens.*, vol. 49, no. 10, pp. 3660–3664, Oct. 2011.

[10] O. Frey, F. Morsdorf, and E. Meier, "Tomographic imaging of a forested area by airborne multi-baseline P-band SAR," *Sensors, Special Issue on Synthetic Aperture Radar*, vol. 8, no. 9, pp. 5884–5896, Sept. 2008.